Conditional Loss of Ikkα in Sp7/osterix+ Cells Has No Effect on Bone, but Leads to Cell Autonomous, Age-related Loss of Peripheral Fat

Jennifer L Davis
Washington University School of Medicine
Nitin K Pokhrel
Washington University School of Medicine
Linda Cox
Washington University School of Medicine
Roberta Faccio
Washington University School of Medicine
Deborah J Veis (dveis@wustl.edu)
Washington University School of Medicine

Research Article

Keywords: Osx-Cre-driven, cKO, Osx-Cre mediated, fat metabolism, peripheral adipocytes

Posted Date: December 9th, 2021

DOI: https://doi.org/10.21203/rs.3.rs-1129360/v1

Abstract

NF-κB has been reported to both promote and inhibit bone formation. To further explore its role in osteolineage cells, we conditionally deleted IKKα, an upstream kinase required for non-canonical NF-κB activation, using Sp7/Osterix (Osx)-Cre. Surprisingly, we found no effect on either cancellous or cortical bone, even following mechanical loading. However, we noted that IKKα conditional knockout (cKO) mice began to lose body weight after 6 months of age with severe reductions in fat mass in geriatric animals. Low levels of recombination at the IKKα locus were detected in fat pads isolated from 15 month old cKO mice. To determine if these effects were mediated by unexpected deletion of IKKα in peripheral adipocytes, we looked for Osx-Cre-mediated recombination in fat using reporter mice, which showed increasing degrees of reporter activation in adipocytes with age up to 18 months. Since Osx-Cre-driven recombination in peripheral adipocytes increases over time, we conclude that loss of fat in aged cKO mice is most likely caused by progressive deficits of IKKα in adipocytes. To further explore the effect of IKKα loss on fat metabolism, we challenged mice with a high fat diet at 2 months of age, finding that cKO mice gained less weight and showed improved glucose metabolism, compared to littermate controls. Thus, Osx-Cre mediated recombination beyond bone, including within adipocytes, should be considered as a possible explanation for extraskeletal phenotypes, especially in aging and metabolic studies.

Introduction

Although NF-κB is primarily considered key to acute inflammatory responses, this is not universally true, particularly for the alternative or non-canonical pathway. Unlike the canonical pathway, which is activated in minutes and generally inactivated within hours, alternative NF-κB is induced over many hours and typically persists for days. NIK functions as a central signaling component in this pathway, orchestrating signals from multiple stimuli and activating downstream kinase IKKα. This triggers phosphorylation of p100 and its partial processing, subsequently leading to persistent activation of the p52/RelB transcriptional complex 1. Besides participating in inflammatory responses due to its activation in immune cells, alternative NF-κB is involved developmentally in lymph node organogenesis, via the stroma 2-4, and plays a cell-extrinsic role in myelopoiesis 5. Expression of NIK in intestinal epithelial cells controls specialized antigen-presenting cells in the gut 6. Outside of its effects on the immune system, alternative NF-κB has been shown to control pathologic angiogenesis via direct actions in endothelial cells 7. Upregulation of NIK in skeletal muscle occurs in patients with metabolic syndrome and decreases with weight loss after gastric bypass 8. Alternative NF-κB also plays a role in metabolism via direct actions in pancreatic beta cells and hepatocytes 9. Thus, there is ample evidence that the alternative NF-κB pathway is important in a variety of cell types and physiologic contexts.

Bone is a dynamic organ, maintained by the coordinated actions of osteoblasts, which produce bone matrix, osteoclasts, which degrade bone, and osteocytes, which act as mechanosensors directing osteoblast and osteoclast activities. Osteocytes differentiate from osteoblasts, and together these cell types comprise the osteolineage. Few studies, all employing global knockout models, have directly addressed the role of alternative NF-κB in osteoblasts 10-13. These displayed complex skeletal

phenotypes, largely pointing to positive effects on bone mass with pathway inhibition. However, we recently explored the role of alternative NF-κB in bone using a constitutively active NIK allele (NT3) lacking a negative regulatory domain, expressed in the osteolineage, finding increased bone mass 14. In contrast, the effect of alternative NF-κB signaling in the osteoclast is well-established. We and others have previously shown that NIK, IKKα, and RelB support osteoclastogenesis, particularly during pathological osteolysis 13,15-20. Due to these direct effects of alternative NF-κB on osteoclasts and physiologic coupling between osteoclasts and osteoblasts, the cell autonomous role of this pathway in osteoblasts remains unclear.

To better understand the role of alternative NF-κB in bone formation, we set out to conditionally inhibit it in osteoblasts. As in the previous study with activated NIK [ref – Davis JBMR], we chose to target early osteoblasts for modulation of alternative NF-κB throughout the lifespan of osteoblasts and osteocytes. The transcription factor Osterix, also known as Sp7, is upregulated as mesenchymal stromal cells become committed to the osteoblast lineage, and in adult mice, its expression in the skeleton is largely confined to osteoblasts and most osteocytes 21,22. Therefore, the Osterix promoter has been widely used to drive Cre expression in many studies of bone 23,24. At the initiation of this study, mice with a conditional allele for deletion of NIK were not yet available, so we employed IKKαfl/fl mice, ablating the second kinase in the alternative NF-κB pathway.

Materials And Methods

Mice

Mice were communally housed in a pathogen-free barrier facility, with controlled temperature and 12-hour light/dark cycles. They had *ad libitum* access to fresh water and standard rodent chow (Purina 5058, St. Louis, MO, USA) unless otherwise indicated. Protocols were approved by Institutional Animal Studies Committee at Washington University School of Medicine (ASC protocols 20170025 and 19-1059) and all methods were performed in accordance with the relevant guidelines and regulations, including with ARRIVE guidelines.

The IKKα flox transgenic line was generated as described elsewhere 40. Osx1-GFP::Cre mice (catalog #006361; The Jackson laboratory, ME USA) express Cre-recombinase under control of a Tet-OFF cassette 23. The IKKα flox transgenic and Osx1-GFP:Cre (Osx-Cre) parental mouse lines were maintained separately due to strain differences (C57Bl/6J and mixed C57Bl/6J and CD1, respectively). Osx-Cre;IKKα$^{fl/fl}$ (cKO) mice and Cre-negative WT;IKKα$^{fl/fl}$ (CON) littermates were maintained on a 200ppm doxycycline chow diet (Purina Test Diet #1816332-203, St. Louis, MO, USA). Pups were switched to standard rodent chow at weaning (P21-P22). To generate TdTomato (TdT) reporter mice, Osx-Cre mice were crossed with TdT mice (catalog #007909; The Jackson Laboratory, ME USA), and pups were maintained on the same doxycycline chow until weaning (P21-P22). Age and sex-matched animals from the same colony were used in all experiments.

Micro-computed tomography

The right tibia of mice was scanned by microCT *in vivo* (VivaCT 40, Scanco, Brüttisellen, Switzerland) at 10.5 mm resolution (70 kVp, 114 mA, 8W, 100ms integration time). Cancellous bone parameters were measured at a 1 mm region distal to the end of the tibial growth plate. Cortical measurements were made at the tibial mid-shaft (1 mm region defined 5 mm proximal to the distal tibiofibular junction). Bone indices are reported in accordance with established standards 41.

Dual-energy X-ray absorptiometry (DXA)

Whole body DXA scans were performed on 18 month male CON and cKO mice using a Faxitron UltraFocus 100 machine (Faxitron, Buffalo Grove, IL, USA).

Mechanical loading and dynamic histomorphometry

Unilateral axial tibial compression (Electropulse 1000; Instron, Norwood, MA, USA) and dynamic histomorphometry (Bioquant Osteo software v18.2.6; Bioquant Image Analysis Corp., Nashville, TN, USA) was performed on the right tibiae of 16-week-old, male mice as previously described 14. The left tibia served as the contralateral non-loaded control. Strain gauging was performed to determine the force necessary for a 2000 microstrain deformation (9.6N, both genotypes). In samples where the mineral apposition rate was zero, an imputed value of 0.1 was used to allow for statistical comparisons. All measurements were acquired in a blinded fashion and reported in accordance with published standards 41.

Genomic DNA recombination

Long bones were flushed of marrow and crushed in TRIzol (15596026; Invitrogen, USA) using a Navy RINO lysis kit and Bullet Blender Tissue Homogenizer (Next Advance, Troy, NY, USA). Peripheral fat depots were processed similarly to crushed bone samples. Cell cultures were rinsed 2x with PBS, then lysed directly in TRIzol. Genomic DNA was extracted using a back extraction buffer (4M guanidine thiocyanate, 50mM sodium citrate, 1M Tris) and alcohol precipitation. 50ng of input gDNA per sample using GoTaq polymerase (M7123, Promega, USA). PCR cycling conditions: 94°C - 4 min; (94°C – 30 sec, 55°C - 45 sec, 72°C – 1.5 min) x 30 cycles; 72°C – 10 min; 12°C hold. Primer sequences for recombination: Forward - CTT TGC CAT CAT CTC TCC GGT TTG TAA; Reverse - CAA TAG GAT AAT CAC TAA GCA CAG T.

High Fat Diet

Mice were fed a 60% kcal/fat diet (#D12492, Research Diets Inc, New Brunswick, NJ, USA), *ad libitum*, beginning at 8-9 weeks of age. Body weight was measured once a week. At sacrifice, peripheral fat pads were weighed after removal of any gross contaminating tissue.

EchoMRI

Lean and fat mass was assessed by EchoMRI body composition analysis (EchoMRI LLC, Houston TX, USA) in non-fasted mice. Each mouse was scanned twice and the average value was used for analysis.

Glucose and insulin tolerance tests

Mice were housed on aspen bedding and administered intraperitoneally a 1mg/g dose of dextrose or 0.75U/kg of insulin (HumulinR U-100, Eli Lily, USA) after a 6h or overnight fast (food only), as indicated. Tail vein blood was sampled at intervals over a 2 hour period and blood glucose was measured using a Bayer Contour meter (#9556C, Bayer HealthCare, Mishawaka, IN, USA) and accompanying test strips.

Immunostaining and Fluorescence Imaging

Inguinal fat was embedded in optimal cutting temperature compound (OCT; 23-730-571, Thermo Fisher Scientific, USA) and flash frozen at -80°C. Embedded tissues were post fixed in 10% neutral buffered formalin and cut at 50 µm on a cryostat (Leica, Buffalo Grove, IL, USA). For immunostaining, cut sections on glass slides were blocked in 10% goat serum in Tris- NaCl- Tween (TNT) buffer before incubation for 24 hours with primary antibodies; anti-perilipin 1 (N-terminus) guinea pig polyclonal (# LS-C665927-100,GP29, LS Bio, USA) (1:1000), anti-CD45 monoclonal antibody (30-F11)(#14-051-82, Thermo Fisher Scientific, USA) (1:200) overnight at 4°C. After washing 3× 5 minutes with TNT, secondary antibodies (Alexa 488 (#A-11073, Thermo Fisher Scientific, USA) or Alexa 488 (#A-48269, Thermo Fisher Scientific, USA) in TNT buffer were applied for 1 hour at room temperature. The sections were then washed 3× 5 minutes in TNT buffer, before mounting with Fluoromount-G (#00-4958-02, Thermo Fisher Scientific, USA). Images were captured using Leica DMi8 automated inverted microscope equipped with ACS APO 20x/0.60 Lens (Leica Microsystems).

Statistical Analysis

All statistics were computed using GraphPad Prism software (Version 9.2.0, GraphPad Software, Inc., La Jolla, CA, USA). Values of $p<0.05$ were considered significant and data are presented as mean ± SD. For pairwise comparisons, either a student's, unpaired, two-tailed t-test or student's paired, two-tailed t-test was used. A Welch's correction was applied to the t-test if the F-test to compare variances was significantly different. For multiple group comparisons, a 2-way ANOVA followed by Tukey's multiple comparison test was performed. For repeated measure group comparisons, a 2-way repeated measures ANOVA followed by Sidak's multiple comparison test was performed. A mixed-effect model was used if sample sizes differed. Specific statistical tests and sample sizes are indicated in the respective figure legends.

Results

Conditional deletion of IKKα in the osteoblast lineage does not alter bone mass

We mated IKKα$^{fl/fl}$ and Osx-cre mice to generate Osx-Cre;IKKα$^{fl/fl}$ (cKO) and Cre-negative (CON) littermates. Dams were kept on doxycycline throughout pregnancy and until pups were weaned to prevent early Cre expression that can impact skeletal growth. Activation of Cre and excision of the floxed IKKα

allele were assessed in bone marrow-derived mesenchymal stromal cell cultures (BMSCs) under osteogenic conditions and in flushed, crushed bones from cKO and CON littermates. Cre expression was undetectable in unstimulated BMSCs and rose during osteogenesis (Fig S1A). Interestingly, however, recombination of the IKKα allele was robust, even prior to addition of osteogenic media (Fig S1B). Importantly, Cre expression and recombination did not occur in CON bones but were readily detected in cKO samples (Fig S1C,D). We next assessed the effect of IKKα deficiency on osteogenesis in vitro and found a modest increase in mineralization as well as expression of osteoblast markers (Fig S2).

We used in vivo microCT to screen for bone effects in male mice at multiple ages and found no differences in cortical or cancellous parameters in the tibia at any time (Fig. 1a,b, S3-6). Aged males were also screened by DXA, but again no differences in bone mass were seen (Fig. 1c). In females, ex vivo microCT at 16 weeks of age also failed to detect bone changes after IKKα deletion (Fig S7). To determine if an anabolic condition would elicit a bone-specific role for IKKα, we applied unilateral tibial compression for 2 weeks in 16 week old male mice. However, again, we saw no differences by genotype (Fig. 2). We therefore concluded that IKKα plays little or no role in osteogenesis in basal or mechanical loading conditions.

Aging IKKα cKO mice lose fat, associated with improved glucose metabolism

As we aged mice to examine their bone phenotype, we noted that the cKO mice appeared smaller. In fact, analysis of body weights showed not only lower weights for the cKO cohorts overall at both 12 and 18 months, but also a 13% decrease in weight in the same animals between 6 and 12 months of age, compared to a 9% increase over the same period in CON (Fig. 3a,b). EchoMRI was then used to quantitate fat and lean mass. cKO mice displayed distinctly lower fat mass at 12 and 18 months (47% and 62% respectively), with a more modest, but still statistically significant, decrease in lean mass (Fig. 3c,d). Post mortem, both gonadal and inguinal fat pads were smaller in cKO than CON mice (Fig. 3e,f).

Because reductions in fat are often accompanied by changes in glucose metabolism, we challenged mice with glucose tolerance testing (GTT) after a 6h fast. At 7-9 mo of age, the response to glucose challenge was nearly identical (Fig. 4a). By middle-age (13-15 mo), cKO mice showed a mild but significant decrease in peak blood glucose levels (Fig. 4b). Old (18-20 mo) cKO animals displayed a trend towards lower peak glucose (Fig. 4c), and this difference was further accentuated after an overnight fast (Fig. 4d), indicating improved glucose tolerance in old cKO mice.

Osx-Cre mediates increasing recombination in adipocytes with age

Based on these changes in fat mass and glucose metabolism, we next sought to determine if the IKKα floxed locus was recombined in cKO fat. We performed PCR to detect the deleted allele in inguinal, gonadal, renal, and brown fat pads and observed the recombination product at multiple sites in cKO animals, but not CON (Fig. 5a). Fat tissue contains many cell types besides adipocytes, including

endothelium and other vascular components, as well as hematopoietic cells such as macrophages. To specifically examine Osx-Cre driven recombination, we examined fat pads from Osx-Cre;TdTomato (TdT) reporter mice raised in the same manner as the IKKα cKO mice, using confocal microscopy. We found limited reporter expression in inguinal fat at 6 and 12 weeks of age, with substantially increased signal at 6 and especially 18 months (Fig. 5b). The pattern of TdT coincided with immunostaining for perilipin, demonstrating that recombination occurs in adipocytes. In contrast, we found no co-staining of TdT with CD45 (Fig. 5c), indicating that recombination in hematopoietic cells in fat is unlikely to be responsible for the observed low-fat phenotype. Based on this data, we conclude that Osx-Cre drives recombination in peripheral adipocytes, in an age-dependent manner.

IKKα cKO mice show a blunted response to high fat diet

To further investigate the fat phenotype observed in aged cKO mice, we deployed a well-established high fat diet (HFD) model in younger animals. Mice were fed this diet (60%kcal/fat) beginning at 8 weeks of age, prior to any difference in body weight between CON and cKO mice (Fig. 6a and S8a). Male cKO mice showed blunted weight gain which did not reach statistical significance following 8 weeks of HFD, although total fat mass was decreased by ECHO MRI (S8). Intriguingly, attenuation of weight gain in female cKO mice was significant (60% increase in CON vs 40% increase in cKO) (Figure 6b), associated with a marked reduction in fat mass (Figure 6c). Total lean mass was unchanged in both sexes, compared to CON (Figure 6d and S8d).

After 8-11 weeks on HFD, male cKO mice showed a trend towards better glucose tolerance, but this did not reach statistical significance in our cohorts (S8d). Glucose tolerance in females after 8-11 weeks similarly trended better in cKO mice (Fig. 7a,b). Insulin tolerance was not significantly different in either sex at this point, although female cKO showed a slight trend towards better tolerance (S8f and Fig. 7c,d). We then decided to continue HFD in a subset of females for 20-23 weeks. After this extended period, body weight continued to be lower in cKO, and both glucose and insulin tolerance were significantly improved compared to CON (Fig. 7e-i). Because significant changes in weight and fat mass occurred long before alterations in glucose metabolism, it is likely that the metabolic effects are secondary to, rather than the primary drivers of, weight gain.

Discussion

In this study, we set out to examine the role of alternative NF-κB signaling in the osteolineage by targeting a key upstream kinase, IKKα, using Osx-cre. Previously, we found that forced activation of this pathway using a constitutively active allele of NIK with the same Osx-cre driver enhanced both basal and stimulated bone formation 14. Here, male cKO mice showed no differences in bone mass up to 18 months of age, and mechanical loading by tibial compression failed to generate any differences in bone formation. Female mice also had normal bone mass at 4 months of age. Thus, under basal and non-inflammatory loading conditions, IKKα does not seem to have a clear role, either positive or negative, in bone formation. One limitation of our bone analysis is that we did not follow females over time, despite our finding that global loss of alternative NF-κB components NIK and RelB has greater effect in females.

However, in those models, the differences are clear by 10 weeks of age. It is possible that IKKα may impact bone formation in the context of strong inflammatory stimuli such as inflammatory arthritis models, which were not examined here.

Although Osx-Cre efficiently drives recombination in osteoblasts, not all phenotypes identified can be attributed to effects in the osteolineage. The Osx-Cre allele has established recombination activity in many extraskeletal tissues including synovium 25, intestinal epithelium 26,27,, and kidney 28, as well as in some hematopoietic stem and progenitor cells 29. In tumor bearing mice, Osterix, as well as the Osx-Cre allele, is also expressed in a subset of cancer-associated fibroblasts with a dual fibroblast/osteogenic signature 29. Recently, we found subcutaneous sarcomas, but not bone tumors, in mice expressing a transgene driven by Osterix-cre 30. Therefore, given the striking loss of fat in aging cKO mice in the absence of any changes in bone, we considered the possibility that recombination outside of bone was responsible for the phenotype. PCR of genomic DNA from peripheral fat depots in middle aged mice showed some recombination of the IKKα allele, albeit less robust than in bone. Examination of inguinal fat pads from reporter mice showed robust TdT expression only in adipocytes from aged mice. Despite identification of TdT in several subsets of CD45+ cells in a previous study using the same line of Osx-Cre;TdT mice 29, we did not identify any such cells in the inguinal fat sections at any age. We therefore concluded that Osx-Cre can drive recombination in adipocytes, and this cell autonomous effect is the most likely cause of the cKO fat phenotype. Future experiments using an adipose-specific cre driver are required to confirm this and would be useful to determine the mechanism by which IKKα impacts adipocyte metabolism.

In addition to the unexpected finding of a fat phenotype driven by Osx-Cre, we also did not anticipate the strong effect of age on activation of this Cre. Previous studies utilizing this Cre driver primarily utilize mice under 6 months of age, and the few studies with mice at or beyond 1 year of age did not describe, or specifically look for, Cre expression outside of bone 31-33. More comprehensive analysis of conditional mouse models with sensitive reporters like TdTomato is likely to uncover other so-called off-target effects that arise with aging in many Cre lines.

Most studies of the role of NF-κB in adipocytes have focused on IKKβ, an apex kinase in the canonical pathway. Loss of IKKβ in mature adipocytes using Adiponectin-Cre or Adipoq-Cre did not affect body weight in normal or HFD conditions 34,35. However, although fat mass was decreased in these models, the mice were insulin resistant on HFD. In contrast, with conditional loss of IKKβ in adipocyte progenitors, lower fat mass on HFD was accompanied by improved glucose homeostasis 36. Constitutive activation of IKKβ in adipocytes prevented diet-induced obesity and improved glucose tolerance 37. Interestingly, IKKβ in adipocytes may act via direct phosphorylation of targets such as β-catenin and BAD 34,38, rather than via activation of canonical NF-κB. Thus, the role of IKKβ in the adipocyte lineage is complex. Furthermore, the effects of aging have not been studied in any of these models.

Data on the role of IKKα or other components of alternative NF-κB in metabolism is even more limited, with effects described in pancreatic islets, hepatocytes, and skeletal muscle 9. However, there has been

an absence of conditional knockout studies for the pathway in peripheral adipocytes. Our cKO model, although not initially designed to target fat or metabolism, nevertheless highlights the importance of IKKα in peripheral fat, both with aging and diet-induced obesity. Whether IKKα in adipocytes acts through alternative NF-κB signaling, via other downstream kinase targets, or in a kinase-independent fashion 39, remains to be established.

Since this study was undertaken to examine the role of IKKα in bone, studies of fat and metabolism were not initially planned. By the time the fat phenotype in aging males was discovered, it was not practical to undertake a similar study in females. Therefore, we decided to investigate whether differences in fat could be accelerated using HFD in both sexes. Interestingly, although both male and female cKO mice had less fat than CON after 8 weeks on the obesogenic diet, the difference in overall body weight was more pronounced in females. Thus, like osteoclasts 13, adipocytes may have differential sensitivity to the alternative NF-κB pathway by sex.

In sum, using an Osx-Cre driven conditional knockout approach, we found no clear role for IKKα in the osteolineage in either basal or mechanically stimulated conditions, but rather an intriguing role for IKKα in fat accumulation with age or diet-induced obesity. Although further experiments specifically targeting adipocytes are needed, the results shown here suggest that inhibition of IKKα, or potentially other alternative NF-κB pathway components, may reduce fat deposition with age and improve glucose metabolism. With increasing recognition of bone as an endocrine organ, it is tempting to conclude that phenotypes arising from conditional alleles driven by Osx-Cre are due to the osteolineage. However, our finding of age-related changes in Osx-Cre expression in peripheral fat indicates that expression outside of bone should be considered when metabolic phenotypes are identified in aged animals.

Declarations

Author contributions

JLD – experimental design, data acquisition, analysis, and interpretation, drafting and revision of manuscript

NKP - data acquisition and analysis, drafting and revision of manuscript

LC – data acquisition

RF – experimental design, data interpretation

DJV – experimental design, data interpretation, drafting and revision of manuscript

Acknowledgements

This work was supported by National Institutes of Health Grants R01 AR052705 and P01 CA100730 (to DJV), R01 AR070030 (to DJV and RF), R01 AR066551 (to RF), and F31 AR068853 and T32 CA113275 (to

JLD). MicroCT and histology services were provided by the Washington University Musculoskeletal Research Center's Structure and Strength and Histology and Morphometry Cores, supported by P30 AR074992. EchoMRI analysis was performed in the Washington University Nutrition Obesity Research Center, supported by P30 DK056341 via a just-in-time grant. Additional support was provided by the Siteman Cancer Center Investment Program, St. Louis, MO to RF. Funding from Shriners Hospitals for Children was provided to DJV and RF. We wish to thank Crystal Idleburg for histological expertise, and Sangeeta Adak, Nidhi Rohatgi, and Erica Scheller for assistance with fat and metabolism experiments.

Competing interests

The authors declare no competing interests.

References

1. Sun, S. C. Non-canonical NF-kappaB signaling pathway. *Cell Res*, **21**, 71–85 https://doi.org/doi:10.1038/cr.2010.177 (2011).
2. Benezech, C. *et al.* Lymphotoxin-beta receptor signaling through NF-kappaB2-RelB pathway reprograms adipocyte precursors as lymph node stromal cells., **37**, 721–734 https://doi.org/doi:10.1016/j.immuni.2012.06.010 (2012).
3. Roozendaal, R. & Mebius, R. E. Stromal cell-immune cell interactions. *Annu. Rev. Immunol*, **29**, 23–43 https://doi.org/doi:10.1146/annurev-immunol-031210-101357 (2011).
4. Weih, F. & Caamano, J. Regulation of secondary lymphoid organ development by the nuclear factor-kappaB signal transduction pathway. *Immunol. Rev*, **195**, 91–105 https://doi.org/doi:10.1034/j.1600-065x.2003.00064.x (2003).
5. Briseno, C. G. *et al.* Deficiency of transcription factor RelB perturbs myeloid and DC development by hematopoietic-extrinsic mechanisms. *Proc Natl Acad Sci U S A*, **114**, 3957–3962 https://doi.org/doi:10.1073/pnas.1619863114 (2017).
6. Ramakrishnan, S. K. *et al.* Intestinal non-canonical NFkappaB signaling shapes the local and systemic immune response. *Nature communications*, **10**, 660 https://doi.org/doi:10.1038/s41467-019-08581-8 (2019).
7. Noort, A. R. *et al.* NF-kappaB-inducing kinase is a key regulator of inflammation-induced and tumour-associated angiogenesis. *J. Pathol*, **234**, 375–385 https://doi.org/doi:10.1002/path.4403 (2014).
8. Choudhary, S. *et al.* NF-kappaB-inducing kinase (NIK) mediates skeletal muscle insulin resistance: blockade by adiponectin., **152**, 3622–3627 https://doi.org/doi:10.1210/en.2011-1343 (2011).
9. Sun, S. C. The non-canonical NF-kappaB pathway in immunity and inflammation. *Nat. Rev. Immunol*, **17**, 545–558 https://doi.org/doi:10.1038/nri.2017.52 (2017).
10. Novack, D. V. *et al.* The IkappaB function of NF-kappaB2 p100 controls stimulated osteoclastogenesis. *J. Exp. Med*, **198**, 771–781 https://doi.org/doi:10.1084/jem.20030116 (2003).

11. Seo, Y. *et al.* Accumulation of p100, a precursor of NF-kappaB2, enhances osteoblastic differentiation in vitro and bone formation in vivo in aly/aly mice. *Mol. Endocrinol*, **26**, 414–422 https://doi.org/doi:10.1210/me.2011-1241 (2012).
12. Yao, Z. *et al.* NF-kappaB RelB negatively regulates osteoblast differentiation and bone formation. *J Bone Miner Res*, **29**, 866–877 https://doi.org/doi:10.1002/jbmr.2108 (2014).
13. Zarei, A. *et al.* Manipulation of the Alternative NF-kappaB Pathway in Mice Has Sexually Dimorphic Effects on Bone. *JBMR plus*, **3**, 14–22 https://doi.org/doi:10.1002/jbm4.10066 (2019).
14. Davis, J. L. *et al.* Conditional Activation of NF-kappaB Inducing Kinase (NIK) in the Osteolineage Enhances Both Basal and Loading-Induced Bone Formation. *J Bone Miner Res*, **34**, 2087–2100 https://doi.org/doi:10.1002/jbmr.3819 (2019).
15. Vaira, S. *et al.* RelB is the NF-kappaB subunit downstream of NIK responsible for osteoclast differentiation. *Proc Natl Acad Sci U S A*, **105**, 3897–3902 https://doi.org/doi:10.1073/pnas.0708576105 (2008).
16. Yang, C. *et al.* NIK stabilization in osteoclasts results in osteoporosis and enhanced inflammatory osteolysis. *PLoS One*, **5**, e15383 https://doi.org/doi:10.1371/journal.pone.0015383 (2010).
17. Zeng, R., Faccio, R., Novack, D. V. & Alternative NF-kappaB Regulates RANKL-Induced Osteoclast Differentiation and Mitochondrial Biogenesis via Independent Mechanisms. *J Bone Miner Res*, **30**, 2287–2299 https://doi.org/doi:10.1002/jbmr.2584 (2015).
18. Chaisson, M. L. *et al.* Osteoclast Differentiation Is Impaired in the Absence of Inhibitor of kB Kinasea. *J. Biol. Chem*, **279**, 54841–54848 (2004).
19. Taniguchi, R. *et al.* RelB-induced expression of Cot, an MAP3K family member, rescues RANKL-induced osteoclastogenesis in alymphoplasia mice by promoting NF-kappaB2 processing by IKKalpha. *J Biol Chem*, **289**, 7349–7361 https://doi.org/doi:10.1074/jbc.M113.538314 (2014).
20. Soysa, N. S. *et al.* The pivotal role of the alternative NF-kappaB pathway in maintenance of basal bone homeostasis and osteoclastogenesis. *J Bone Miner Res*, **25**, 809–818 https://doi.org/doi:10.1359/jbmr.091030 (2010).
21. Nakashima, K. *et al.* The novel zinc finger-containing transcription factor osterix is required for osteoblast differentiation and bone formation., **108**, 17–29 https://doi.org/doi:10.1016/s0092-8674(01)00622-5 (2002).
22. Baek, W. Y. *et al.* Positive regulation of adult bone formation by osteoblast-specific transcription factor osterix. *J Bone Miner Res*, **24**, 1055–1065 https://doi.org/doi:10.1359/jbmr.081248 (2009).
23. Rodda, S. J. & McMahon, A. P. Distinct roles for Hedgehog and canonical Wnt signaling in specification, differentiation and maintenance of osteoblast progenitors. *Development*, **133**, 3231–3244 https://doi.org/doi:10.1242/dev.02480 (2006).
24. Elefteriou, F. & Couasnay, G. Advantages and Limitations of Cre Mouse Lines Used in Skeletal Research. *Methods Mol. Biol*, **2230**, 39–59 https://doi.org/doi:10.1007/978-1-0716-1028-2_3 (2021).
25. Miura, Y., Ota, S., Peterlin, M., McDevitt, G. & Kanazawa, S. A. Subpopulation of Synovial Fibroblasts Leads to Osteochondrogenesis in a Mouse Model of Chronic Inflammatory Rheumatoid Arthritis.

JBMR plus, **3**, e10132 https://doi.org/doi:10.1002/jbm4.10132 (2019).

26. Chen, J. *et al.* Osx-Cre targets multiple cell types besides osteoblast lineage in postnatal mice. *PLoS One*, **9**, e85161 https://doi.org/doi:10.1371/journal.pone.0085161 (2014).
27. Wang, L. *et al.* SHP2 regulates the development of intestinal epithelium by modifying OSTERIX(+) crypt stem cell self-renewal and proliferation. *FASEB J*, **35**, e21106 https://doi.org/doi:10.1096/fj.202001091R (2021).
28. Strecker, S., Fu, Y., Liu, Y. & Maye, P. Generation and characterization of Osterix-Cherry reporter mice. *Genesis (New York, N.Y.*: 2000) **51**, 246-258, doi:10.1002/dvg.22360 (2013)
29. Ricci, B. *et al.* Osterix-Cre marks distinct subsets of CD45- and CD45+ stromal populations in extra-skeletal tumors with pro-tumorigenic characteristics. *eLife*, **9**, https://doi.org/doi:10.7554/eLife.54659 (2020).
30. Davis, J. L. *et al.* Constitutive activation of NF-kappaB inducing kinase (NIK) in the mesenchymal lineage using Osterix (Sp7)- or Fibroblast-specific protein 1 (S100a4)-Cre drives spontaneous soft tissue sarcoma. *PLoS One*, **16**, e0254426 https://doi.org/doi:10.1371/journal.pone.0254426 (2021).
31. Ng, A. J. *et al.* The DNA helicase recql4 is required for normal osteoblast expansion and osteosarcoma formation. *PLoS Genet*, **11**, e1005160 https://doi.org/doi:10.1371/journal.pgen.1005160 (2015).
32. Zannit, H. M. & Silva, M. J. Proliferation and Activation of Osterix-Lineage Cells Contribute to Loading-Induced Periosteal Bone Formation in Mice. *JBMR plus*, **3**, e10227 https://doi.org/doi:10.1002/jbm4.10227 (2019).
33. Pierce, J. L. *et al.* The glucocorticoid receptor in Osterix-expressing cells regulates bone mass, bone marrow adipose tissue, and systemic metabolism in female mice during aging. *J Bone Miner Res*, https://doi.org/doi:10.1002/jbmr.4468 (2021).
34. Park, S. H. *et al.* IKKbeta Is Essential for Adipocyte Survival and Adaptive Adipose Remodeling in Obesity., **65**, 1616–1629 https://doi.org/doi:10.2337/db15-1156 (2016).
35. Kwon, H. *et al.* Adipocyte-specific IKKbeta signaling suppresses adipose tissue inflammation through an IL-13-dependent paracrine feedback pathway. *Cell reports*, **9**, 1574–1583 https://doi.org/doi:10.1016/j.celrep.2014.10.068 (2014).
36. Helsley, R. N. *et al.* Targeting IkappaB kinase beta in Adipocyte Lineage Cells for Treatment of Obesity and Metabolic Dysfunctions., **34**, 1883–1895 https://doi.org/doi:10.1002/stem.2358 (2016).
37. Jiao, P. *et al.* Constitutive activation of IKKbeta in adipose tissue prevents diet-induced obesity in mice., **153**, 154–165 https://doi.org/doi:10.1210/en.2011-1346 (2012).
38. Sui, Y. *et al.* IKKbeta is a beta-catenin kinase that regulates mesenchymal stem cell differentiation. *JCI insight*, **3**, https://doi.org/doi:10.1172/jci.insight.96660 (2018).
39. Liu, F., Xia, Y., Parker, A. S. & Verma, I. M. IKK biology. *Immunol. Rev*, **246**, 239–253 https://doi.org/doi:10.1111/j.1600-065X.2012.01107.x (2012).

40. Liu, B. *et al.* IKKalpha is required to maintain skin homeostasis and prevent skin cancer., **14**, 212–225 https://doi.org/doi:10.1016/j.ccr.2008.07.017 (2008).
41. Dempster, D. W. *et al.* Standardized nomenclature, symbols, and units for bone histomorphometry: a 2012 update of the report of the ASBMR Histomorphometry Nomenclature Committee. *J Bone Miner Res*, **28**, 2–17 https://doi.org/doi:10.1002/jbmr.1805 (2013).

Figures

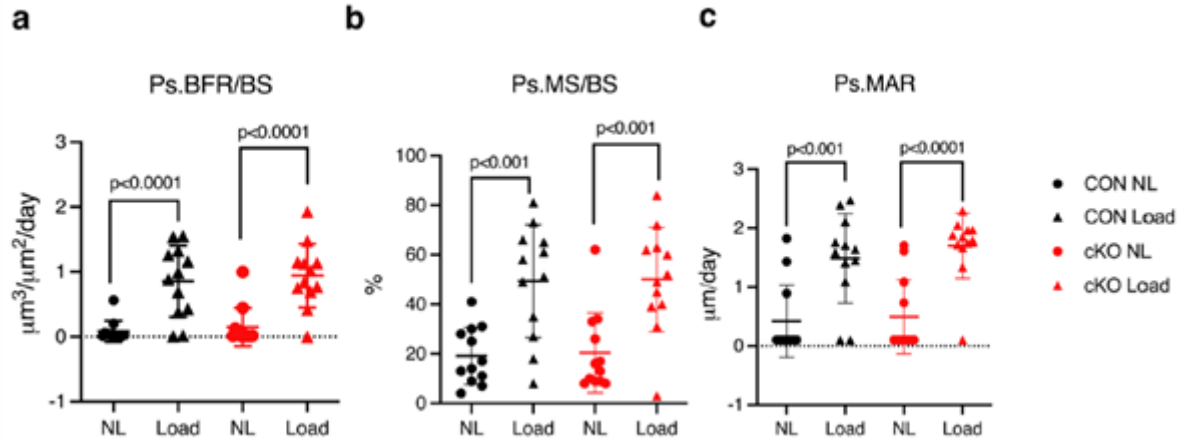

Figure 1

IKKα cKO mice have similar basal bone mass compared to controls. a) Cancellous bone volume fraction (BV/TV) or b) Cortical thickness (Ct.Th) of tibiae at 6 wks (n=12), 12 wks (n=11-13), 6 mo (n=11), 12 mo (n=11) by in vivo microCT. c) Whole body bone mineral density by dual-energy x-ray absorptiometry (DXA) for 18-20 mo mice (n=11). Data are represented as mean SD. CON = black circles, cKO = red triangles, all male mice. Non-significant between genotypes at each age by student's, unpaired, two-tailed t-test.

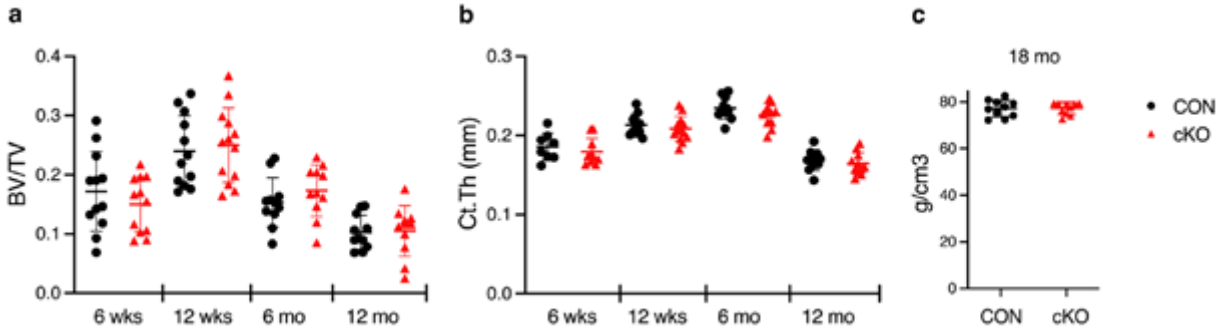

Figure 2

IKKα cKO mice have a similar response to anabolic loading compared to control. Anabolic response to unilateral axial tibial compression was assessed by dynamic histomorphometry, measuring parameters along the periosteum (Ps) after 2 wks. a) Bone formation rate per bone surface (Ps.BFR/BS), b) Mineralizing surface per bone surface (Ps.MS/BS), and c) Mineral apposition rate (Ps.MAR). CON = black,

cKO = red, all male mice. Right tibiae were loaded (Load, triangles) and left tibiae served as non-loaded (NL, circles) controls. Results are presented as mean SD. n=12 per genotype. 2-way ANOVA followed by Tukey's multiple comparison test; response to load within genotypes. There were no significant differences between genotypes, or interactions between genotype and loading.

Figure 3

IKKα cKO mice have attenuated weight gain, lower total fat, and less lean mass with age. a) Body weights at 6 mo (n=15-16), 12 mo (n=28-31), 18 mo (n=11-13). b) Weight change (%) from 6 mo to 12 mo (n=11). EchoMRI measurement of c) total fat mass and d) total lean mass at 6mo (n=6), 12mo (n=5-9), 18mo (n=10-11). e) Gonadal and f) Inguinal fat pad weights at 12 mo (n=4-9) and 18 mo (n=11-14). Data are represented as mean SD, all male mice. CON = black, cKO = red. Student's, unpaired, two-tailed t-test (For b) or 1-way ANOVA (cross genotype comparisons): ns – non-significant.

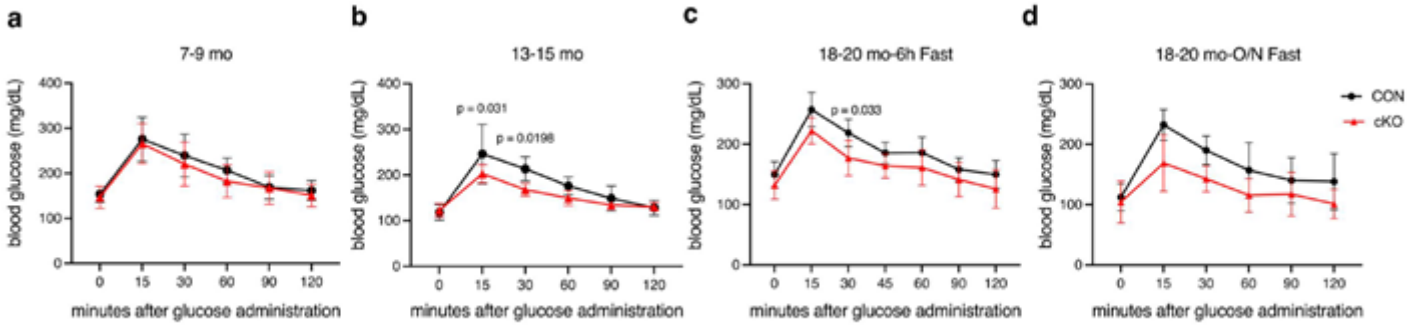

Figure 4

Older IKKα cKO mice show improved glucose tolerance. Glucose Tolerance Test (GTT) was performed after a 6h fast at all ages and overnight (O/N) at 18-20 mo. CON = black, cKO = red, all male mice. Blood glucose measurements at a) 7-9 mo (n=7-9), b) 13-15 mo (n=5-6), c) 18-20 mo (n=4-7), and d) 18-20 mo after O/N fast (n=4-7). Data are represented as mean SD. Repeated measures 2-way ANOVA followed by Sidak multiple comparisons test, with p values indicated where significant.

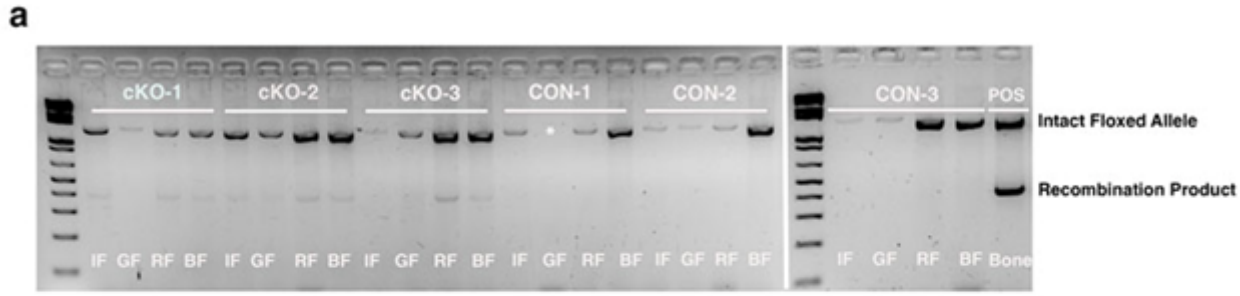

Figure 5

Osx-Cre mediates recombination in peripheral adipocytes. (a) PCR of genomic DNA from inguinal fat (IF), gonadal fat (GF), renal fat (RF), and brown fat (BF), isolated from 15 mo male mice. Whole, flushed bone was used as a positive control (POS). Intact floxed allele = 1.3kb and recombination product = 460bp. *, sample lost in loading. Right panel was originally on the bottom row of the same gel as the left panel. n=3 biological replicates. Representative immunofluorescence staining for (b) Perilipin (green) or (c) CD45 (green) in inguinal fat from Osx-Cre;TdT reporter mice (red) at 6 wks, 12 wks, 6 mo, 18 mo, or Osx-Cre- control mice at 18 mo.

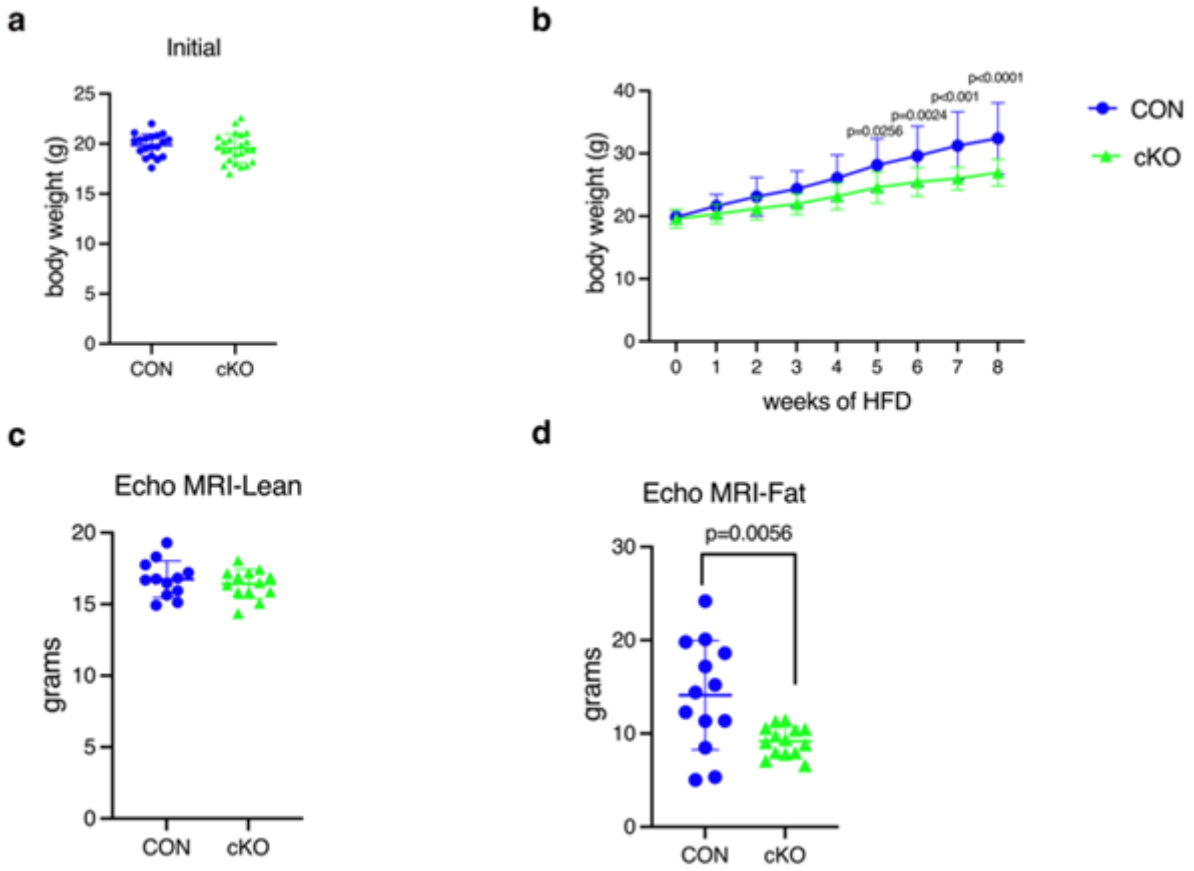

Figure 6

IKKα cKO mice show blunted weight and fat gain after HFD. Body weights (BW), a) Initial or b) after HFD for 8 wks. CON = blue, cKO = green. c) EchoMRI of total fat mass or d) total lean mass after 8wks on HFD. Data are represented as mean SD. Female mice (initial BW, n=15-23; HFD BW, n=12-18; EchoMRI, n=10-14). Repeated measures 2-way ANOVA followed by Sidak multiple comparisons test for body weight on HFD for b and Student's, unpaired, two-tailed t-test for a,c,d and e. HFD = high fat diet.

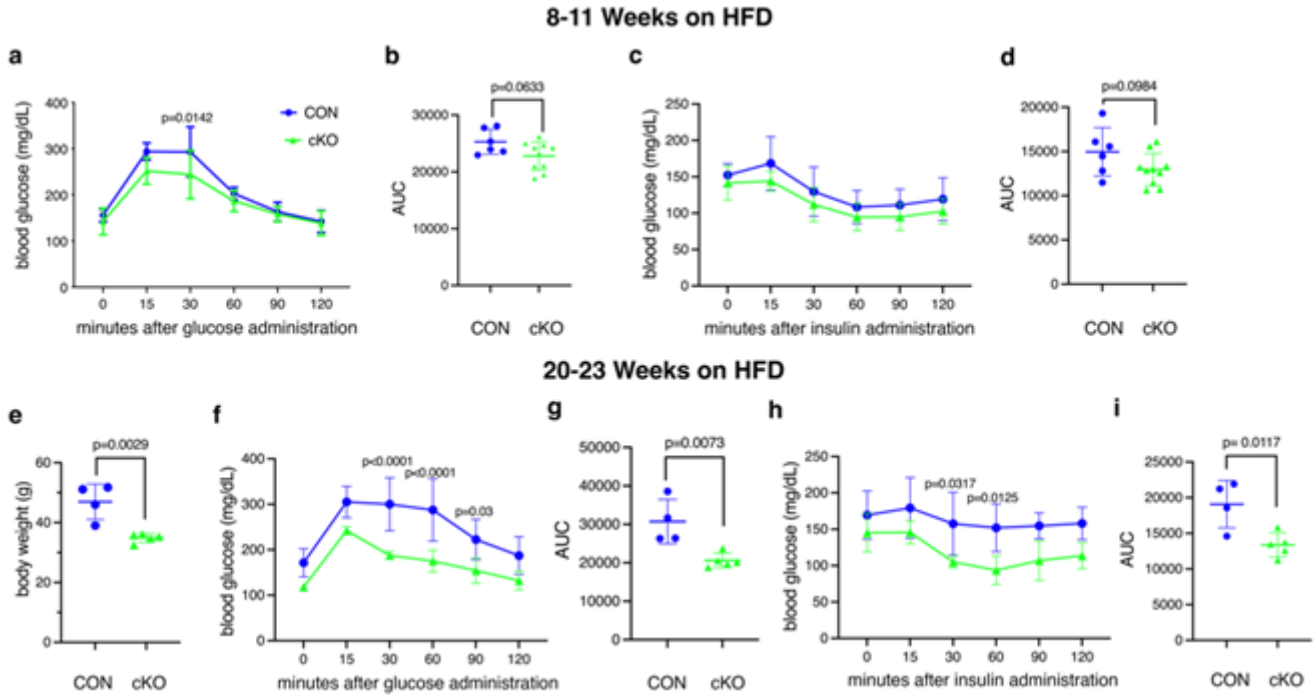

Figure 7

IKKα cKO mice show improved glucose metabolism after HFD. Blood glucose levels were measured during Glucose Tolerance Tests (GTT) and Insulin Tolerance Tests (ITT), which were initiated after a 6h fast, in female mice. a-d) Tests were performed after 8-11 wks on HFD (n=6-10). a) GTT, b) area under the curve (AUC) for GTT, c) ITT, and d) AUC for ITT. e-i) Tests were repeated on a subset of mice after 20-23 wks on HFD (n=4-6). e) body weight at time of GTT, f) GTT, g) AUC for GTT, h) ITT, and i) AUC for ITT. CON = blue, cKO = green. Data are represented as mean SD. Repeated measures 2-way ANOVA followed by Sidak multiple comparisons test for GTT and ITT or Student's, unpaired, two-tailed t-test for body weight and AUC.

Supplementary Files

This is a list of supplementary files associated with this preprint. Click to download.

- IKKAlphaSupplementaryfinalwithgels.pdf